

# Sparse Identification for Data-Driven Dynamics and Impedance Modeling of Power Converters in DC Microgrids

Ali Hosseini-pour, *Student member, IEEE.*, and Javad Khazaei, *Senior Member, IEEE.*

**Abstract**—Confidentiality and variability of the parameters of power converters motivate applying system identification in power electronic systems. In this paper, a novel identification framework based on the sparse regression technique is proposed for DC-DC converters operating in a microgrid in order to derive the nonlinear dynamics of the converter under test (CUT) for data-driven control and to estimate the small-signal impedance of the CUT for online stability analysis purposes. The CUT is perturbed by swept-sine and pseudo-random binary sequence (PRBS) excitation signals via an external source in order to collect dynamically-rich time- and frequency-domain measurements during the online operation of the CUT. The measurements are then fed to an optimization problem solved by the sequential thresholded least squares (STLS) algorithm to discover the nonlinear averaged dynamics and the sparse parameter-varying (SPV) impedance model of the CUT. The data-driven controllers designed using the identified dynamics are shown to exhibit close performance to their physics-based counterparts. Furthermore, the SPV impedance model is also shown to accurately track the measured impedance of the CUT and obviates the need for continuous perturbation of the system at each operating point. Real-time simulation results and frequency-domain analyses are presented to verify the effectiveness of the proposed framework.

**Index Terms**—dc-dc converter, DC microgrid, real-time identification, sparse regression, dynamical modeling, droop control, small-signal impedance model.

## I. INTRODUCTION

Modeling of DC distribution systems and microgrids is typically conducted assuming the full knowledge of analytical models of switch-mode power converters, also referred to as white-box models [1]. However, with the proliferation of commercial off-the-shelf converters, detailed information about converter parameters is usually not available [2]. Moreover, the dynamics of power converters are subject to change due to aging [3] and faults [4], which motivates utilizing system identification techniques by leveraging measurement data [5]. Identified dynamic models of power converters can be used to design data-driven control [6] and development of digital twins [7], [8] for online stability and condition monitoring of power electronic systems.

Identification of power converters can be conducted by black-box and grey-box modeling techniques. Linear black-box methods typically make use of the two-port model of

power converters to approximate transfer functions at fixed operating points [9], [10]. Linear models are, however, limited to applications such as small-signal analysis [11]. Being an integral part of DC distribution systems, DC-DC converters have been studied for nonlinear dynamics identification using polytopic [12]–[14] and Hammerstein [15], [16] black-box methods. Both Hammerstein and polytopic methods still rely on linear methods to estimate nonlinear dynamics, which renders them operating-point-dependent and thus unable to represent full non-linear dynamics. Non-linear black-box modeling methods based on wavelet and dynamic artificial neural networks (ANNs) are proposed in [1], [17], respectively. However, the main drawbacks of ANN-based identification methods are computational cost, requirement for large number of training data points, and the lack of physical interpretability.

On the other hand, grey-box identification methods rely on the partial knowledge of the system model, which then serves as a foundation to estimate a complete model [18]. Grey-box identification of DC-DC buck converters using the NARMAX model is discussed in [19], [20] by using *a priori* knowledge of the static behavior of the converter. In [21], the prediction capability of the grey-box methods proposed in [19], [20] is improved by incorporating *a priori* knowledge of the converter static behavior in the structure selection of the model using the NARX technique. However, only the identification of voltage dynamics is addressed in [19]–[21] rather than a complete dynamic model. In [7], grey-box modeling using an iterative least-squares technique is conducted for a half-bridge converter to discover its state-space dynamic model. A prior knowledge of state-space equations and nominal parameters of the converter are required, which are not always accessible. A hybrid Wiener-Hammerstein grey-box modeling technique is also proposed in [22], which relies on the information provided in the data sheet of converters to predict the large-signal behavior, power consumption, and efficiency of DC-DC converters. In [23], a physics-informed deep neural network is proposed for estimating the parameters of a DC-DC buck converter. The method assumes prior knowledge of the parametric dynamic equations of the converter and also suffers from high computational costs and long training times.

Small-signal output impedance of power converters is also a valuable parameter to represent the converter dynamics [24], making the impedance-based stability analysis the most common method for online stability monitoring of power electronic systems and microgrids [25]. In order to obtain the real-time impedance, the majority of online stability analysis tools

This research was in part under support from the National Science Foundation under Grant NSF-EPCN 2221784. The authors are with the Department of Electrical and Computer Engineering at Lehigh University, Bethlehem, PA 18015 USA. (E-mails: alh621@lehigh.edu, khazaei@lehigh.edu)

rely on perturbing the converter using wide- or narrow-band signals. Wide-band perturbation is used in [26] to measure the voltage loop gain and equivalent bus impedance of a DC microgrid. Online stability monitoring of a DC microgrid by measuring the output impedance of power converters is proposed in [27]. In [28], an impedance estimation method is proposed, which requires control loop measurement using the Middlebrook's analog injection technique, which is only capable of estimating the impedance around the peak frequency. Vector fitting is also commonly used as a technique to fit the frequency-domain measurements to a linear parametric impedance model [29]. The aforementioned impedance derivation methods are all based on measuring the small-signal impedance of the power converter at each operating point of the system, which requires continually perturbing the system. Imposing frequent perturbations to the system is considered invasive and computationally intensive in addition to not being ideal for online stability monitoring purposes where run-time efficiency is of great importance. Recent studies have tackled the operating-point dependency of small-signal impedance models for inverter-based resources using ANNs [30], [31]. However, the main drawback of ANNs for this purpose is the requirement for large amount of data since these methods use the frequency as one of the inputs of the ANN impedance predictor.

To bridge the gap in the studies reviewed above, here an identification framework based on the sparse regression technique [32] is proposed for DC-DC converters. A half-bridge DC-DC converter operating under droop control in a microgrid is considered as the converter under test (CUT). In the proposed framework, the nonlinear dynamics of the CUT are directly discovered from a library of candidate functions by solely relying on measurement data that are available as the feedback signals of the CUT's control system. It is shown in Table I that the proposed method is not only independent of linear models, but also results in closed-form dynamics with minimum prior knowledge of the CUT. Furthermore, the sparse regression technique is applied to estimate the parametric output impedance model of the CUT, resulting in the sparse parameter-varying (SPV) impedance model. The SPV impedance model obviates the need to conduct a frequent perturbation of the system for the purpose of real-time impedance measurement, improving the run-time efficiency of impedance identification and reducing the computational burden of online stability monitoring tools. Table II demonstrates the advantages of the SPV impedance model over the state-of-the-art methods in the sense that it is operating-point independent and does not require frequency data points as an input to the model in the training stage.

The major contributions of the paper include:

- The nonlinear averaged dynamics of the CUT are identified by a sparse identification framework from dynamically-rich data collected during the online operation of the CUT in a microgrid. The performance of the data-driven controllers corresponding to the identified dynamics are then assessed.
- A data-driven parametric impedance model called the SPV impedance is proposed to estimate the closed-loop

output impedance of the CUT. The SPV impedance model obviates the need to perform a continuous perturbation of the system for the purpose of online impedance measurement and is shown to achieve an estimation time 10 times faster than the estimation time of the full nonlinear dynamics.

The rest of the paper is organized as follows. Section II introduces the theory of sparse identification. In Section III, the identification of nonlinear dynamics of the CUT is discussed. In Section IV, the concept of data-driven SPV impedance using the proposed framework is presented. Various real-time case studies are provided in Section V to assess the performance of the proposed identification frameworks in time and frequency domains. Section VI concludes the paper.

## II. SPARSE IDENTIFICATION OF NONLINEAR DYNAMICS OF NON-HOMOGENEOUS SYSTEMS

The underlying principle of the sparse identification method is that non-homogeneous dynamical systems of the form  $\dot{\mathbf{x}} = \mathbf{f}(\mathbf{x}, \mathbf{u})$ , given in (1), typically have only a few terms on the right-hand side of their state-space model [32].

$$\frac{d}{dt}\mathbf{x}(t) = \dot{\mathbf{x}}(t) = \mathbf{f}(\mathbf{x}(t), \mathbf{u}(t)) \quad (1)$$

where  $\mathbf{x}(t) \in \mathbb{R}^n$  is the state vector,  $\mathbf{u}(t) \in \mathbb{R}^q$  is the input or control vector, and  $\mathbf{f}(\mathbf{x}(t), \mathbf{u}(t)) : \mathbb{R}^n \times \mathbb{R}^q \rightarrow \mathbb{R}^n$ .

The function  $\mathbf{f}$  only consists of few active terms from the space of possible right-hand side functions. The possible right-hand side terms can be represented by a library of candidate functions,  $\Theta \in \mathbb{R}^{m \times p}$ , required for approximation of the dynamics of  $\mathbf{f}$ . This library comprises a total of  $p$  candidate terms, typically including linear and nonlinear monomials of  $\mathbf{x}$  and  $\mathbf{u}$  and usually a constant term as well. In order to evaluate  $\Theta$ ,  $m$  time-series snapshots of the state  $\mathbf{x}$  and the input  $\mathbf{u}$  are collected either through simulations or experiments. Then, they are arranged into matrices of the forms

$$\mathbf{X} = \begin{bmatrix} \cdot & \cdot & \cdot & \cdot & \cdot & \cdot \\ \cdot & \cdot & \cdot & \cdot & \cdot & \cdot \\ \cdot & \cdot & \cdot & \cdot & \cdot & \cdot \\ \cdot & \cdot & \cdot & \cdot & \cdot & \cdot \\ \cdot & \cdot & \cdot & \cdot & \cdot & \cdot \\ \cdot & \cdot & \cdot & \cdot & \cdot & \cdot \end{bmatrix}^T \quad (2)$$

$$\mathbf{U} = \begin{bmatrix} \cdot & \cdot & \cdot & \cdot & \cdot & \cdot \\ \cdot & \cdot & \cdot & \cdot & \cdot & \cdot \\ \cdot & \cdot & \cdot & \cdot & \cdot & \cdot \\ \cdot & \cdot & \cdot & \cdot & \cdot & \cdot \\ \cdot & \cdot & \cdot & \cdot & \cdot & \cdot \\ \cdot & \cdot & \cdot & \cdot & \cdot & \cdot \end{bmatrix}^T \quad (3)$$

Therefore, for a system with  $n$  states,  $q$  inputs, and  $m$  time-series snapshots of data,  $\mathbf{X}$  and  $\mathbf{U}$  can be written as

$$\mathbf{X} = \begin{bmatrix} \cdot & \cdot & \cdot & \cdot & \cdot & \cdot \\ \cdot & \cdot & \cdot & \cdot & \cdot & \cdot \\ \cdot & \cdot & \cdot & \cdot & \cdot & \cdot \\ \cdot & \cdot & \cdot & \cdot & \cdot & \cdot \\ \cdot & \cdot & \cdot & \cdot & \cdot & \cdot \\ \cdot & \cdot & \cdot & \cdot & \cdot & \cdot \end{bmatrix} = \begin{bmatrix} \mathbf{x}^T(t_1) & x_1(t_1) & x_2(t_1) & \dots & x_n(t_1) \\ \mathbf{x}^T(t_2) & x_1(t_2) & x_2(t_2) & \dots & x_n(t_2) \\ \cdot & \cdot & \cdot & \cdot & \cdot \\ \cdot & \cdot & \cdot & \cdot & \cdot \\ \mathbf{x}^T(t_m) & x_1(t_m) & x_2(t_m) & \dots & x_n(t_m) \end{bmatrix} \quad (4)$$

$$\mathbf{U} = \begin{bmatrix} \cdot & \cdot & \cdot & \cdot & \cdot & \cdot \\ \cdot & \cdot & \cdot & \cdot & \cdot & \cdot \\ \cdot & \cdot & \cdot & \cdot & \cdot & \cdot \\ \cdot & \cdot & \cdot & \cdot & \cdot & \cdot \\ \cdot & \cdot & \cdot & \cdot & \cdot & \cdot \\ \cdot & \cdot & \cdot & \cdot & \cdot & \cdot \end{bmatrix} = \begin{bmatrix} \mathbf{u}^T(t_1) & u_1(t_1) & u_2(t_1) & \dots & u_q(t_1) \\ \mathbf{u}^T(t_2) & u_1(t_2) & u_2(t_2) & \dots & u_q(t_2) \\ \cdot & \cdot & \cdot & \cdot & \cdot \\ \cdot & \cdot & \cdot & \cdot & \cdot \\ \mathbf{u}^T(t_m) & u_1(t_m) & u_2(t_m) & \dots & u_q(t_m) \end{bmatrix} \quad (5)$$

TABLE I: State-of-the-art research on nonlinear model identification of power converters.

Reference	Method	Linear-model independent	Closed-form identification	Prior-knowledge independent
[12]–[14]	Polytopic	×	×	✓
[15], [16]	Hammerstein	×	×	✓
[1], [17]	Neural Network	✓	×	✓
[19], [20]	NARMAX	✓	×	×
[21]	NARX	✓	×	×
[22]	Wiener-Hammerstein	×	×	×
[7]	Iterative Least-squares	✓	✓	×
[23]	Physics-informed Neural Network	✓	×	×
Proposed	Sparse Identification	✓	✓	✓

TABLE II: State-of-the-art impedance identification methods for power converters.

Reference	Method	Operating-point independent	Frequency-independent training
[29]	Vector Fitting	×	N/A
[30]	Neural Network	✓	×
[31]	Physics-informed Neural Network	✓	×
Proposed	SPV Impedance	✓	✓

The collected state and input measurements are then compiled into the library  $\Theta$  as given in (6), where higher order polynomials are denoted by functions  $\mathbf{P2}$ ,  $\mathbf{P3}$ , etc. For example,  $\mathbf{P2}(\mathbf{X}, \mathbf{U})$  denotes the quadratic nonlinearities of states and inputs as given in (7).

As can be seen in (6), the library of candidate functions can include constant, polynomial and trigonometric terms. A general guideline is to first include simple functions such as polynomials, and then add more complex terms such as trigonometric functions to the library. However, considering the grey-box nature of the identification method, partial knowledge of the dynamical system can also be leveraged to decide what functions to include in the library [33].

$$\mathbf{P2}(\mathbf{X}, \mathbf{U}) = \begin{bmatrix} x_1(t_1)u_1(t_1) & x_1(t_1)u_2(t_1) & \dots & x_n(t_1)u_q(t_1) \\ x_1(t_2)u_1(t_2) & x_1(t_2)u_2(t_2) & \dots & x_n(t_2)u_q(t_2) \\ \vdots & \vdots & \ddots & \vdots \\ x_1(t_m)u_1(t_m) & x_1(t_m)u_2(t_m) & \dots & x_n(t_m)u_q(t_m) \end{bmatrix}. \quad (7)$$

The obtained data matrices can then be used to represent the dynamical system of (1) as

$$\dot{\mathbf{X}} = \Theta(\mathbf{X}, \mathbf{U})\Xi \quad (8)$$

where  $\Xi$  is the matrix of coefficients for the candidate functions in  $\Theta$ . The derivative matrix  $\dot{\mathbf{X}}$  can also be written in its general form as

$$\dot{\mathbf{X}} = \begin{bmatrix} \dot{x}_1(t_1) & \dot{x}_2(t_1) & \dots & \dot{x}_n(t_1) \\ \dot{x}_1(t_2) & \dot{x}_2(t_2) & \dots & \dot{x}_n(t_2) \\ \vdots & \vdots & \ddots & \vdots \\ \dot{x}_1(t_m) & \dot{x}_2(t_m) & \dots & \dot{x}_n(t_m) \end{bmatrix} = \begin{bmatrix} \mathbf{x}^T(t_1) & \mathbf{x}^T(t_2) & \dots & \mathbf{x}^T(t_m) \end{bmatrix} \begin{bmatrix} x_1(t_1) & x_2(t_1) & \dots & x_n(t_1) \\ x_1(t_2) & x_2(t_2) & \dots & x_n(t_2) \\ \vdots & \vdots & \ddots & \vdots \\ x_1(t_m) & x_2(t_m) & \dots & x_n(t_m) \end{bmatrix}. \quad (9)$$

#### A. Estimating the time derivative matrix $\dot{\mathbf{X}}$

Computation of the time derivative of the state matrix,  $\dot{\mathbf{X}}$ , is required to complete the data collection for the identification process. Considering a smooth function in the neighborhood of a point, the derivatives can be accurately approximated

using Taylor series expansion at specified mesh points. The derivative matrix can be approximated by the central difference method as

$$\dot{\mathbf{X}} \approx \frac{8\mathbf{X}(t_{i+1}) - 8\mathbf{X}(t_{i-1}) + \mathbf{X}(t_{i-2}) - \mathbf{X}(t_{i+2})}{12h} \quad (10)$$

where  $\mathbf{X}(t_i)$  is the time-series sample  $i$  and  $h$  is the mesh spacing, which is considered the same as the simulation sample time used for collecting the data.

#### B. Identification by Sparse Regression

In the final step of the identification process, a sparse regression problem is formulated to solve for the sparse vectors of coefficients in  $\Xi$ , which determine what terms are active in the  $\dot{\mathbf{X}}$  dynamics. The goal of sparse identification is to arrive at the fewest terms in  $\Xi$  that result in a good fit for the collected data from the dynamical system. This is achieved by solving an optimization of the form

$$\hat{\xi}_h = \arg \min_{\xi_h} \|\mathbf{X}_h - \Theta(\mathbf{V}_o, \mathbf{I}_L)\xi_h\|_2 + \lambda \|\xi_h\|_0 \quad (11)$$

where  $\xi_h$  is the  $h$ -th column of  $\Xi$  represented by  $\xi_h = [\xi_{h1} \ \xi_{h2} \ \dots \ \xi_{hp}]^T$ .  $\mathbf{X}_h$  represents the  $h$ -th column of  $\dot{\mathbf{X}}$ . The objective function in (11) comprises two norm functions. The  $\ell_2$  norm denoted by  $\|\cdot\|_2$  solves for the least-squares problem. The  $\ell_0$  norm,  $\|\cdot\|_0$ , decides the number of nonzero elements in  $\xi_h$ , promoting sparsity in the coefficients matrix.

The sparsity-promoting hyperparameter is represented by  $\lambda_h$ . The minimization problem of (11) is approximately solved by the sequential thresholded least squares (STLS) proposed in [32]. The STLS is an iterative algorithm that according to [34] is defined by

$$S^k = \{j \in [p] : \xi_j^k \geq \lambda\}, \quad k \geq 0 \quad (12)$$

$$\hat{\xi}_h^0 = \Theta(\mathbf{V}_o, \mathbf{I}_L)^\dagger \mathbf{X}_h \quad (13)$$

$$\hat{\xi}_h^{k+1} = \underset{\xi_h \in \mathbb{R}^p : \text{supp}(\xi_h) \subseteq S^k}{\text{argmin}} \|\mathbf{X}_h - \Theta(\mathbf{V}_o, \mathbf{I}_L)\xi_h\|_2, \quad k \geq 0 \quad (14)$$



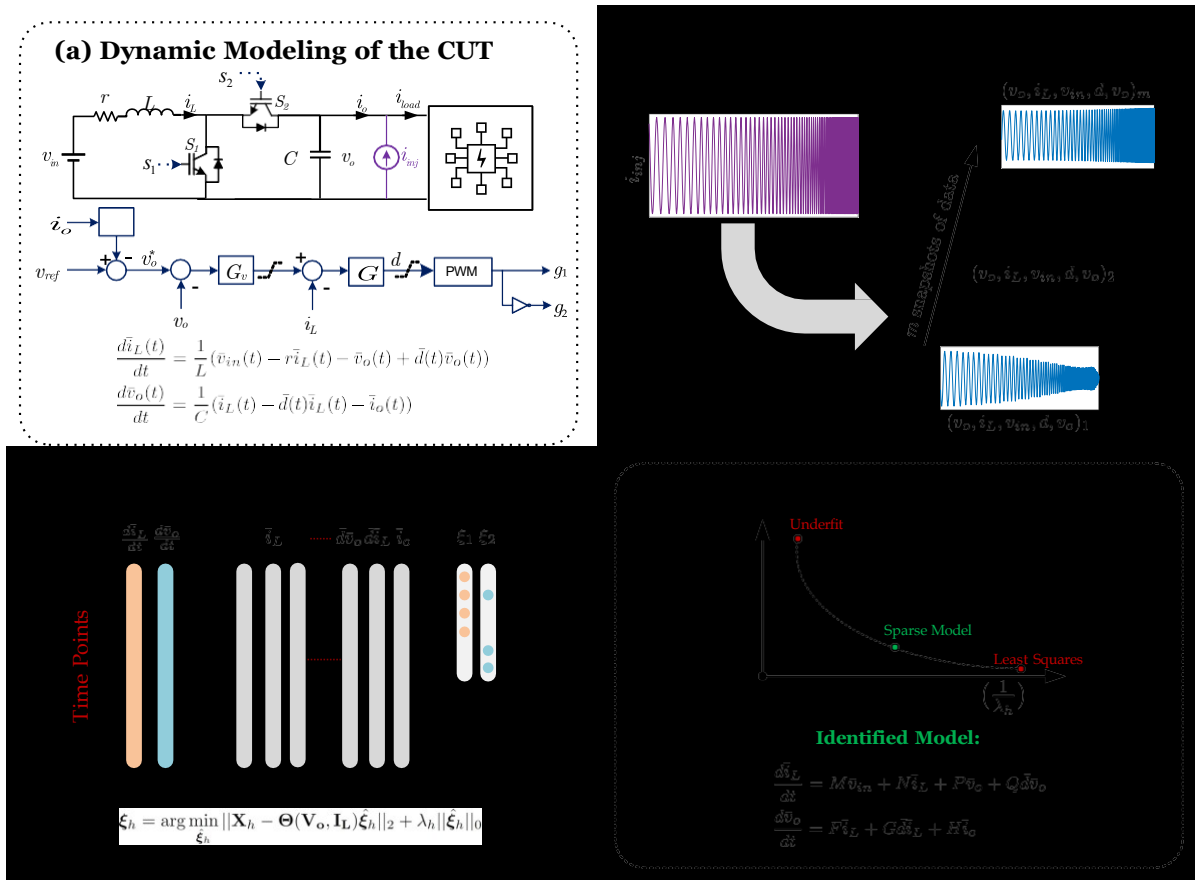


Fig. 1: Sparse identification framework for the identification of the CUT. (a) closed-loop dynamic model of the CUT. (b) data collection by the injection of a swept-sine signal. (c) building the library of candidate functions and applying the sparse regression. (d) discovery of the CUT dynamics by tuning the sparsity-promoting coefficient  $\lambda_h$ .

where  $v_{ref}$  is the nominal output voltage and  $Z_o$  is the droop gain. The droop gain is typically decided by the permissible voltage variations and the converter rating [36].

### C. Data Collection

1) *System excitation*: The next step in the identification process is to collect measurement data. To this end, the system should be excited by an identification signal. In this study, an external current source is used to perturb the CUT at its various operating points with a swept-sine signal,  $i_{inj}$ , as shown in Fig. 1(a). The swept-sine signal is a sequence of sinusoidal signals with different frequencies that are applied successively [37]. The amplitude of the swept-sine should be selected such that the system is not significantly perturbed as it is being tested online. At the same time, it has to be large enough to generate rich data for identification purposes. The advantage of the proposed excitation approach is that it can be performed without perturbing the converter control signals or interrupting the system. The parameters of the swept-sine signal are given Table III. The excitation frequencies are logarithmically spaced between the minimum and maximum frequencies of the swept-sine signal. The frequency range of perturbations is selected so that a sweep up to half of the switching frequency is realized and very low frequencies are also excluded to reduce the measurement time.

TABLE III: Parameters of the swept-sine signal.

Parameter	Value
Number of frequencies	30
Minimum frequency	100 Hz
Maximum frequency	10 kHz
Sample time	10 $\mu$ s
Amplitude (peak-to-peak)	$0.05 \times  i_o $

2) *Averaged values measurement*: It is obvious from (16) and (17) that the state and input measurements of the CUT have to be the averaged values of switching waveforms of the CUT for inclusion in the library of candidate terms. The moving average operator of (26) can be directly applied to the measurements of  $v_{in}$ ,  $i_L$ ,  $v_o$  for this purpose.

$$\bar{x}(t) = \frac{1}{T} \int_{t-T}^t x(\tau) d\tau \quad (26)$$

where  $x(t)$  is the variable to be averaged, and  $T$  is the switching period of the CUT. The averaged duty cycle  $\bar{d}$  is also derived by averaging the gate pulse function of the lower switch in Fig. 1(a). However,  $i_o$  should not be directly computed by applying (26) since it might affect the perturbation signal frequency content. Instead,  $i_o$  is calculated by

$$\bar{i}_{load} - \bar{i}_{inj}.$$

3) *Sparse representation of dynamics*: Next step is to decide the library of candidate terms  $\Theta$ . The choice of the library of candidate terms mainly has minimum dependence on the expert's knowledge of the system, which will be further discussed in section V-A. As depicted in Fig. 1(c), the candidate terms can be various monomial combinations of  $\bar{v}_{in}$ ,  $\bar{i}_L$ ,  $\bar{v}_o$ , and  $\bar{d}$ . Before applying the sparse identification technique, the collected data should be grouped into training and testing datasets. The STLS algorithm is then executed for different values of  $\lambda_h$ , starting from zero up to the value that results in a sparse dynamic model with the minimum cross-validated error according to Fig. 1(d). The resultant identified dynamical equations are

$$\frac{d\bar{i}}{dt} = M\bar{v}_{in} + N\bar{i}_L + P\bar{v}_o + Q\bar{d} + R\bar{i}_o + S\bar{d} + T\bar{d}\bar{i}_o + U\bar{d}\bar{v}_{in} + V\bar{d}\bar{i}_L \quad (27)$$

$$\frac{d\bar{v}_o}{dt} = F\bar{i}_L + G\bar{d}\bar{i}_L + H\bar{i}_o + I\bar{d} + J\bar{v}_{in} + K\bar{v}_o + L\bar{d}\bar{v}_{in} + B\bar{d}\bar{v}_o + E\bar{d}\bar{i}_o \quad (28)$$

where  $M, N, P, Q, R, S, T, U, V, F, G, H, I, J, K, L, B,$  and  $E$  are the estimated scalar coefficients. In order to assess the identified model in the frequency domain, the estimated open-loop transfer functions of the CUT, which are denoted by a hat sign, can also be obtained by substituting the coefficients  $M, N, P, Q, F, G, H$  from (27) and (28) in (16) and (17) and linearizing the equations, which results in

$$\hat{Z}_{out}(s) = \frac{-\tilde{v}_o \mathbf{I}}{\tilde{i}_L} \Big|_{\tilde{v}_{in}, \tilde{d}=0} = \frac{-H(s-N)}{\Delta} \quad (29)$$

$$\hat{G}_{id}(s) = \frac{\tilde{i}_L}{\tilde{d} \mathbf{I}} \Big|_{\tilde{v}_{in}, \tilde{i}_o=0} = \frac{QV_o s + G I_L (P + QD)}{\Delta} \quad (30)$$

$$\hat{G}_{vd}(s) = \frac{\tilde{v}_o \mathbf{I}}{\tilde{d} \mathbf{I}} \Big|_{\tilde{v}_{in}, \tilde{i}_o=0} = \frac{QV_o(F + GD) + G I_L (s - N)}{\Delta} \quad (31)$$

$$\hat{A}_{io}(s) = \frac{-\tilde{i}_L \mathbf{I}}{\tilde{i}_L \mathbf{I}} \Big|_{\tilde{v}_{in}, \tilde{d}=0} = \frac{-H(P + QD)}{\Delta} \quad (32)$$

$$\Delta = s^2 - Ns - (P + QD)(F + GD) \quad (33)$$

where the tilde sign represents small-signal values.

#### IV. SPARSE IDENTIFICATION OF CLOSED-LOOP IMPEDANCE

The estimated closed-loop output impedance of the CUT can be obtained as in (34) using the open-loop transfer functions obtained from the estimated averaged dynamics of the CUT. However, it is still required to have the transfer functions of the controllers, i.e.,  $G_v(s)$  and  $G_d(s)$ , as well as the droop gain  $Z_v$ , in order to obtain the parametric impedance model  $\hat{Z}_{ocl}(s)$  in (34). Moreover, estimating the full nonlinear dynamics of the system may not be required in applications such as online stability monitoring as the closed-loop output impedance of the converters provides enough information about the stability of the system. Readers can refer to [25], [38] for more information about impedance-based stability analysis methods in power electronic systems.

TABLE IV: Parameters of the PRBS excitation signal

Parameter	Value
Signal order	18
Sampling time	10 $\mu$ s
No. of periods	1
Amplitude (peak-to-peak)	$0.05 \times  i_o $

In this section, an impedance estimation framework based on the sparse regression technique is proposed to obtain the SPV impedance model. Using the data-driven SPV impedance model, the parametric closed-loop output impedance of the CUT is learned from the frequency-domain impedance data measured at different operating points of the CUT. The obtained SPV impedance will then be able to predict the small-signal impedance of the CUT at each operating point without the need to measure the impedance at each operating point by continuously perturbing the CUT.

#### A. Impedance Data Collection

Frequency scanning is utilized to collect impedance data at multiple operating points of the CUT. To this end, the system is first initialized at a specific operating point. Then the CUT is excited by PRBS-driven external current source ( $\bar{i}_{inj}$ ) at its output terminals as shown in Fig. 2. The parameters of the PRBS signal are designed such that a sweep up to half of the switching frequency of the CUT is ensured. The designed parameters are given in Table IV.

Next, the impedance frequency-response data is obtained by performing fast Fourier transform (FFT) as

$$Z_{frd}(s) = \frac{F[v_o(t)]}{F[-i_o(t)]} \quad (35)$$

In order to obtain the parametric model of the measured impedance in the frequency domain, a transfer function with four poles and three zeros is fitted to the impedance frequency response data using the vector fitting method embedded in the MATLAB<sup>®</sup> function `tfest`, resulting in  $Z_{meas}(s)$  for a specific operating point of the CUT.

$$Z_{meas}(s) = \frac{b_3 s^3 + b_2 s^2 + b_1 s + b_0}{s^4 + a_3 s^3 + a_2 s^2 + a_1 s + a_0} \quad (36)$$

The impedance data is collected at  $m$  different operating points of the CUT for the training of the sparse regression algorithm discussed next.

#### B. SPV Impedance Model

It can be observed from (29)-(33) that the analytical impedance model of the CUT in (34) is a function of the operating point specified by  $I_L$ ,  $V_o$ , and  $D$ . Since  $D$  can be represented as a function of  $V_o$  and  $I_L$ , the  $(I_L, V_o)$  pair suffices to represent the operating point of the CUT. Therefore, the SPV impedance model,  $Z_{SPV}(s)$ , of the CUT can be



$$\Theta(\mathbf{V}_o, \mathbf{I}_L) = \begin{bmatrix} 1 & \mathbf{V}_o & \mathbf{I}_L & \mathbf{V}_o \mathbf{I}_L & \mathbf{V}_o^2 & \mathbf{I}_L^2 & \mathbf{V}_o^2 \mathbf{I}_L & \mathbf{I}_L^2 \mathbf{V}_o & \mathbf{V}_o^3 & \mathbf{I}_L^3 & \mathbf{V}_o^3 \mathbf{I}_L & \mathbf{V}_o^3 \mathbf{I}_L^2 & \mathbf{I}_L^3 \mathbf{V}_o & \mathbf{I}_L^3 \mathbf{V}_o^2 \end{bmatrix} \quad (40)$$

$m \times p$

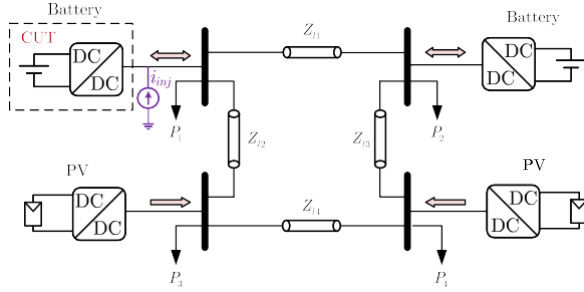


Fig. 3: Implemented DC microgrid for dynamics identification of the CUT.

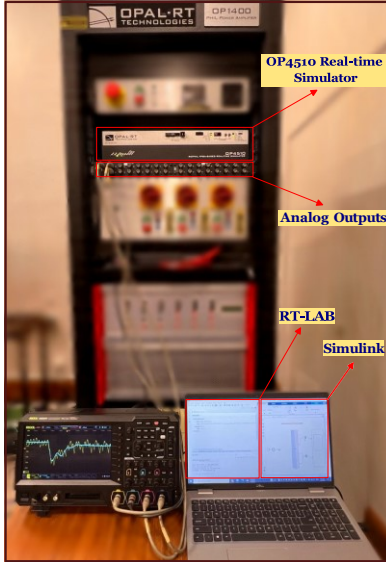


Fig. 4: Real-time simulation setup used for verification.

testing set containing unseen data and the cross validation error (CVE) is computed by

$$\text{CVE} = \frac{\|\mathbf{X}'_{test} - \Theta_{test}(\mathbf{X}, \mathbf{U})\xi_h\|_2}{\|\mathbf{X}'_{test}\|_2} \quad (43)$$

where  $\mathbf{X}'_{test}$  and  $\mathbf{X}_{test}$  are the derivative and state matrices for the testing set, respectively. The CVE is calculated to obtain identification error for both  $i_L$  ( $\text{CVE}_{i_L}$ ) and  $v_o$  ( $\text{CVE}_{v_o}$ ) dynamics. As shown in Table VI, Model I achieves very small estimation errors for both  $i_L$  and  $v_o$  dynamics, whereas Model II-A yields a relatively larger identification error. This larger error is caused by the choice of a larger library of candidate functions. However, it can be seen that Model II-B, which is trained by a larger training dataset, improves the estimation error of Model II-A significantly.

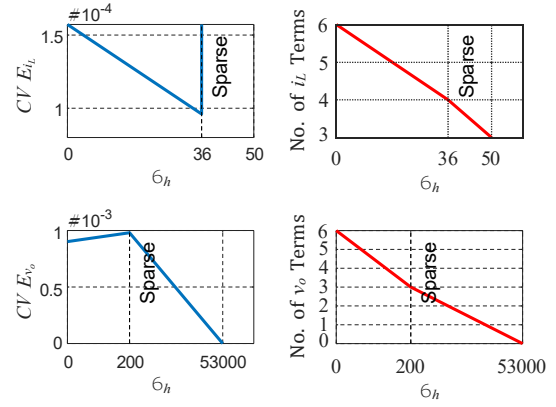


Fig. 5: Sparse model derivation by tuning  $\lambda_h$ .

TABLE V: Simulation parameters of the CUT.

Parameter	Value
Sample time	10 $\mu$ s
$v_{in}$	250 V
$v_{ref}$	380 V
$L$	2.7 mH
$C$	18.953 $\mu$ F
$r$	0.1 $\Omega$
$Z_v$	3.45 $\Omega$
$k_{pvs}, k_{iv}$	0.0339, 25.4
$k_{pis}, k_{ii}$	0.0723, 527
Switching frequency	20 kHz

The procedure for regularization factor ( $\lambda_h$ ) tuning is illustrated in Fig. 5 for Model I, where  $\lambda_h$  is gradually increased from zero (the least-squares solution) until the sparsity is realized for the dynamical equations of  $i_L$  and  $v_o$ . It can be seen that at the sparse point, the dynamical equations have fewer active library functions  $\Theta_1$  than they have when  $\lambda_h=0$ . A further increase in  $\lambda_h$  results in an increase in  $\text{CVE}_{i_L}$  and results in zero coefficients for all candidate functions from  $\Theta_1$  in the case of identification of  $v_o$  dynamics. Therefore,  $\lambda_h=36$  and  $\lambda_h=200$  result in sparse models close to the ground truth dynamics for  $i_L$  and  $v_o$ , respectively.

1) *Performance under small-signal disturbance*: The identified nonlinear dynamic model of the CUT using Model I is compared with the analytical model in Fig. 6. At  $t=0.015$  s, a white noise perturbation is applied to the input voltage to emulate the volatility of the input source. It can be seen that the inductor current exhibits higher frequency variations compared to the capacitor voltage. However, the identified model is able to closely follow the analytical values of the state variables for both the capacitor voltage and inductor current.



TABLE VI: Identified dynamic models of the CUT compared with the analytical model under droop control.

Parameter	Analytical Model	Model I	Model II-A	Model II-B
$M$	370.3704	368.3827	354.2964	373.4869
$N$	-37.037	-37.6831	0	-42.5468
$P$	-370.3704	-368.2940	-362.2083	-372.3595
$Q$	370.3704	368.1235	377.3022	370.1900
$R$	0	0	0	0
$S$	0	0	0	0
$T$	0	0	0	0
$U$	0	0	0	0
$V$	0	0	0	0
$F$	52762	52988	53339	53117
$G$	-52762	-53086	-54363	-53451
$H$	-52762	-52938	-52871	-52962
$I$	0	0	0	0
$J$	0	0	0	0
$K$	0	0	0	0
$L$	0	0	0	0
$B$	0	0	0	0
$E$	0	0	0	0
$CVE_{i_L}$	N/A	$9.6 \times 10^{-5}$	0.0081	$6.78 \times 10^{-5}$
$CVE_{v_o}$	N/A	$9.8 \times 10^{-4}$	0.0026	$6.21 \times 10^{-4}$

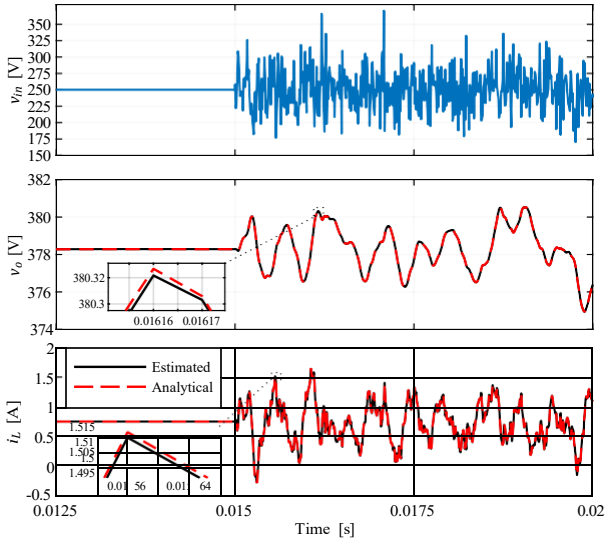


Fig. 6: Analytical dynamic response of the CUT compared with the estimated model under disturbances.

2) *Performance under large-signal disturbance:* Another case study is conducted to evaluate the performance of Model I under large-signal perturbations such as a fault, as depicted in Fig. 7. A large step increase in the output current of the CUT is applied at  $t=0.03$  s to emulate a single line-to-ground fault on the DC bus. The fault clearance is emulated by applying a step decrease in the output current after 3 milliseconds. The identified model can be seen to closely follow the oscillations observed during the fault.

3) *Frequency-domain verification:* The closed-loop output impedance of the CUT derived in (34) is compared for the

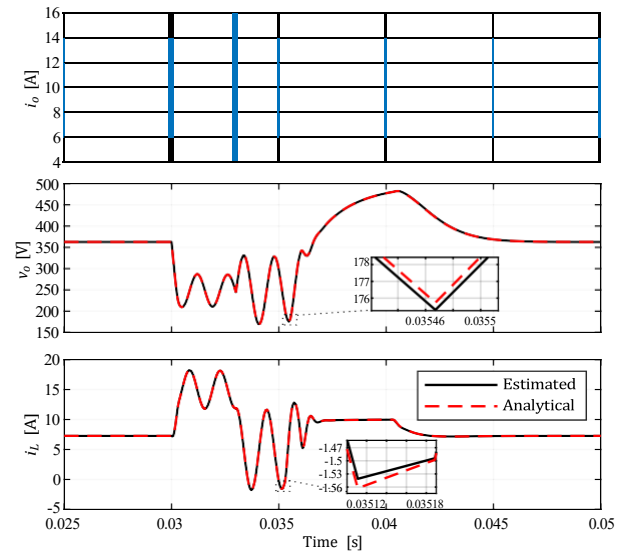


Fig. 7: Analytical dynamic response of the CUT compared with the estimated model under fault conditions.

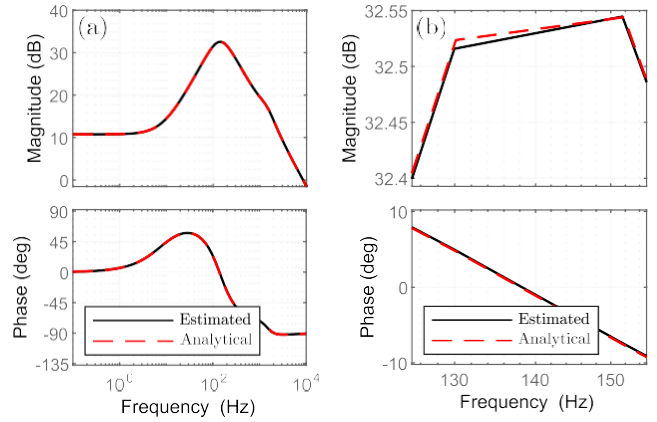


Fig. 8: Closed-loop output impedance of the CUT.

analytical model and Model I in Fig. 8.(a) and Fig. 8.(b). It can be seen that the closed-loop impedance estimated from the identified model closely tracks its analytical counterpart in the entire frequency range without any major inconsistency.

4) *Performance of learning-based controllers:* The estimated dynamics using Model I are utilized to update the voltage and current controller gains of the CUT. The learning-based voltage controller,  $\hat{G}_v(s)$ , and current controller,  $\hat{G}_i(s)$ , are designed based on the same criteria mentioned in Section III-B, but using the estimated dynamics. For this purpose,  $G_{id}(s)$  and  $G_{vd}(s)$  in (21) and (22) are substituted with their estimated counterparts derived in (30) and (31). The obtained gains for the learning-based controllers are calculated as in Table VII. Comparing these gains to the original ones given in Table V, it can be seen that the learned controller gains closely match the original ones. Fig. 9 shows the simulation results when a 500 W step increase in  $P_1$  is applied at  $t=1.2$  s. It can be seen that the learning-based controllers exhibit close performance to the original controllers, proving the capability of the identification framework to adaptively

TABLE VII: Learning-based controllers gains.

Parameter	Value
$k_{pv}, k_{iv}$	0.0337, 25.2
$k_{pi}, k_{ii}$	0.0735, 537.2

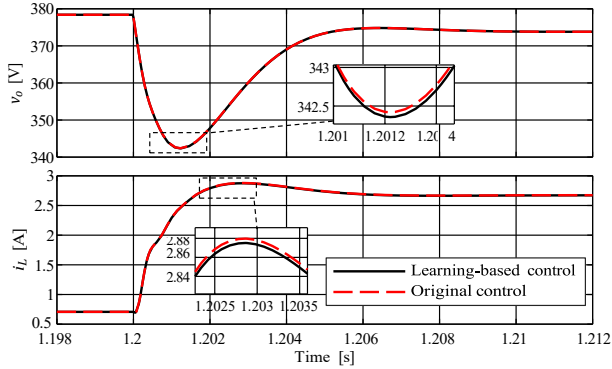


Fig. 9: Performance of learning-based controllers against the original controllers.

tune the controllers based on the identified dynamics of the CUT.

5) *Performance against the switching model:* A step change of 4 A is applied to the CUT's local load in order to analyze the transient performance of Model I against the switching model of the CUT. The capacitor voltage and inductor current waveforms obtained from the identified model and detailed switching model are compared in Fig. 10 and Fig. 11. The identified model (red curves) can be seen to closely follow the moving-averaged dynamics of the switching signals (blue curves). The underdamped oscillations are also clearly reflected by the identified averaged signals.

6) *Identification under constant voltage control:* In order to verify the generalizability of the proposed identification framework under different control techniques, the identification process is conducted on the CUT, but under constant voltage control by setting the droop gain,  $Z_v$ , to zero. The swept-sine perturbation signal,  $\hat{i}_{nj}$ , is injected at various steady-state operating points of the CUT. Similar to the droop-controlled case in Section V-A, the identified models using  $\Theta_1$  and  $\Theta_2$  are referred to as Model I and Model II. Table VIII

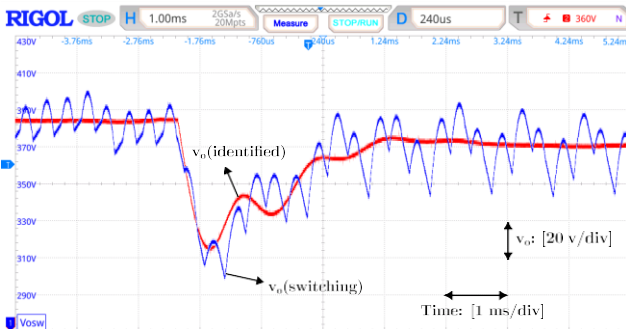


Fig. 10: Identified dynamic model of the output voltage compared with the switching model.

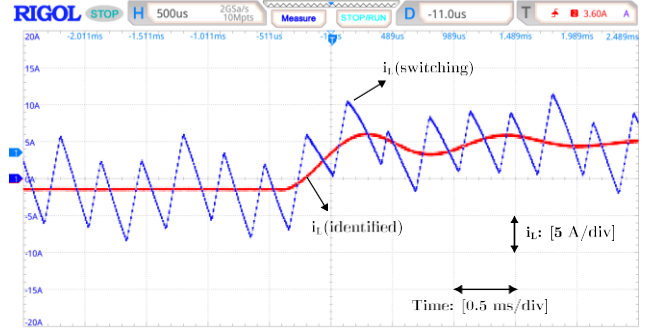


Fig. 11: Identified dynamic model of the inductor current compared with the switching model.

TABLE VIII: Identified dynamic models of the CUT compared with the analytical model under constant voltage control.

Parameter	Analytical Model	Model I	Model II-A	Model II-B
$M$	370.3704	373.8207	353.4154	373.7065
$N$	-37.037	-42.5127	0	-42.1288
$P$	-370.3704	-372.7137	-361.71161	-372.6794
$Q$	370.3704	370.5844	377.6432	370.7027
$R$	0	0	0	0
$S$	0	0	0	0
$T$	0	0	0	0
$U$	0	0	0	0
$V$	0	0	0	0
$F$	52762	53224	53224	53059
$G$	-52762	-53900	-53900	-53160
$H$	-52762	-52913	-52913	-53012
$I$	0	0	0	0
$J$	0	0	0	0
$K$	0	0	0	0
$L$	0	0	0	0
$B$	0	0	0	0
$E$	0	0	0	0
$CVE_{i_L}$	N/A	$4.32 \times 10^{-5}$	0.001	$4.9 \times 10^{-5}$
$CVE_{v_o}$	N/A	$4.34 \times 10^{-4}$	$4.34 \times 10^{-4}$	$3.57 \times 10^{-4}$

compares the coefficients of the nonlinear terms in (27) and (28) for the analytical model with Model I, Model II-A, and Model II-B. Model I and Model II-A are obtained by swept-sine perturbation at 16 different  $V_{ref}$  values for the CUT as the the training data, while Model II-B is trained using data collected from the perturbation at 30 different  $V_{ref}$  values.

Table VIII shows that Model I achieves very small  $CVE_{i_L}$  and  $CVE_{v_o}$ , whereas Model II-A yields a larger  $CVE_{i_L}$  as it is not able to identify the coefficient  $N$ , which is much smaller than other coefficients present in the dynamical equation of  $\hat{i}_L$ . However, Model II-B, trained by a larger training dataset, improves the estimation error of Model II-A significantly. This is verified in Fig. 12 by comparing the estimated dynamics using Model II-B against the ground truth dynamics when the CUT is supplying a constant current load under constant voltage control mode.

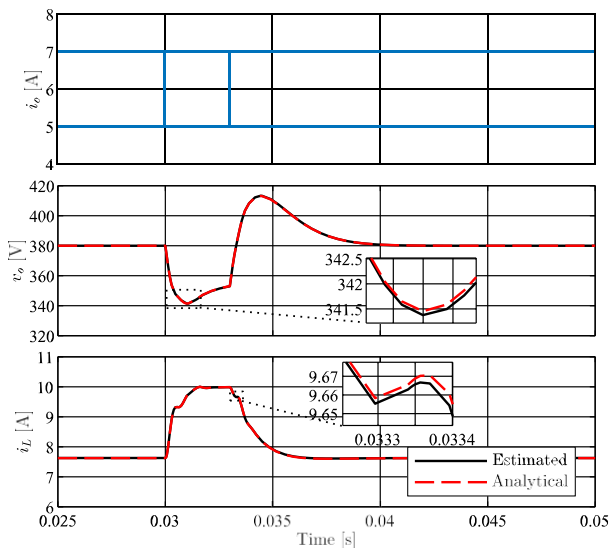


Fig. 12: Analytical dynamic response of the CUT compared with the estimated model under constant voltage control.

### B. SPV Impedance Model Validation

Following the data-driven framework in Fig. 2, the impedance data of 90 different operating points ( $m = 90$ ) are measured through perturbing the CUT with the PRBS signal. The collected data is then split such that 65 randomly selected data points are assigned to the training set and the remaining 25 data points are used for testing. The results of identification is shown in Table IX. It can be observed that the number of active terms for each estimated coefficient function is smaller than the number of candidate terms in (40), verifying the realization of sparsity. The total estimation time for the SPV impedance model is calculated to be 0.0103 seconds, excluding its training time. This is almost 10 times faster than the time for identifying the full dynamic model of the CUT and is thus a more suitable approach for online stability analysis purposes.

The SPV impedance constructed using the estimated coefficient functions in Table IX is compared with the analytical impedance model in Fig. 13 at three distant operating points of the CUT selected from the testing set to illustrate its operating-point independence feature. Fig. 13 shows that the SPV impedance model closely fits its analytical counterpart over the entire frequency range. The maximum identification error occurs mostly at higher frequencies and around the resonant frequencies as shown in Fig. 14.

## VI. CONCLUSION

A sparse identification framework is proposed to identify the averaged nonlinear dynamics and small-signal output impedance of droop-controlled DC-DC converters operating in a microgrid. It is shown that by exciting the CUT by swept-sine and PRBS signals, dynamically-rich data can be collected to identify the nonlinear dynamics and small-signal impedance of the CUT, respectively. The identified dynamic model and small-signal impedance are verified in both time and frequency domains and shown to exhibit a close fit to

their analytical counterparts. Furthermore, the data-driven controllers developed using the identified model also show close performance to their physics-based counterparts. The identified small-signal impedance referred to as the SPV impedance model will enable fast estimation of the impedance at each operating point, which will assist with real-time impedance-based stability monitoring of DC-DC converters in microgrids by avoiding continuous perturbations conventionally used to measure the small-signal impedance.

## REFERENCES

- [1] G. Rojas-Duen˜as, J.-R. Riba, and M. Moreno-Eguilaz, "Black-box modeling of dc-dc converters based on wavelet convolutional neural networks," *IEEE Trans. Instrum. Meas.*, vol. 70, pp. 1–9, 2021.
- [2] A. France's-Roger, A. Anvari-Moghaddam, E. Rodr'iguez-D'iaz, J. C. Vasquez, J. M. Guerrero, and J. Uceda, "Dynamic assessment of cots converters-based dc integrated power systems in electric ships," *IEEE Trans. Ind. Informat.*, vol. 14, no. 12, pp. 5518–5529, 2018.
- [3] J. Hannonen, J. Honkanen, J.-P. Str˜om, T. Ka˜rkk˜ainen, P. Silventoinen, and S. Ra˜isa˜nen, "Capacitor aging detection in dc-dc converter output stage," in *2015 IEEE Energy Conversion Congress and Exposition (ECCE)*, 2015, pp. 5538–5545.
- [4] H. Givi, E. Farjah, and T. Ghanbari, "A comprehensive monitoring system for online fault diagnosis and aging detection of non-isolated dc-dc converters' components," *IEEE Trans. Power Electron.*, vol. 34, no. 7, pp. 6858–6875, 2019.
- [5] M. Al-Greer, M. Armstrong, M. Ahmeid, and D. Giaouris, "Advances on system identification techniques for dc-dc switch mode power converter applications," *IEEE Trans. Power Electron.*, vol. 34, no. 7, pp. 6973–6990, 2019.
- [6] E. Mohammadi, M. Alizadeh, M. Asgarimoghaddam, X. Wang, and M. G. Sim˜oes, "A review on application of artificial intelligence techniques in microgrids," *IEEE J. Emerg. Sel. Topics Ind. Electron.*, vol. 3, no. 4, pp. 878–890, 2022.
- [7] A. Wunderlich, K. Booth, and E. Santi, "Hybrid analytical and data-driven modeling techniques for digital twin applications," in *2021 IEEE Electric Ship Technologies Symposium (ESTS)*, 2021, pp. 1–7.
- [8] S. Zhang, T. Liang, and V. Dinavahi, "Hybrid ml-ent-based digital twin for device-level hil real-time emulation of ship-board microgrid on fpga," *IEEE J. Emerg. Sel. Topics Ind. Electron.*, vol. 4, no. 4, pp. 1265–1277, 2023.
- [9] L. Arnedo, D. Boroyevich, R. Burgos, and F. Wang, "Un-terminated frequency response measurements and model order reduction for black-box terminal characterization models," in *2008 Twenty-Third Annual IEEE Applied Power Electronics Conference and Exposition*, 2008, pp. 1054–1060.
- [10] I. Cvetkovic, D. Boroyevich, P. Mattavelli, F. C. Lee, and D. Dong, "Un-terminated small-signal behavioral model of dc-dc converters," *IEEE Trans. Power Electron.*, vol. 28, no. 4, pp. 1870–1879, 2013.
- [11] B. He, W. Chen, X. Ruan, X. Zhang, Z. Zou, and W. Cao, "A generic small-signal stability criterion of dc distribution power system: Bus node impedance criterion (bnic)," *IEEE Trans. Power Electron.*, vol. 37, no. 5, pp. 6116–6131, 2022.
- [12] L. Arnedo, D. Boroyevich, R. Burgos, and F. Wang, "Polytopic black-box modeling of dc-dc converters," in *2008 IEEE Power Electronics Specialists Conference*, 2008, pp. 1015–1021.
- [13] A. France's, R. Asensi, and J. Uceda, "Blackbox polytopic model with dynamic weighting functions for dc-dc converters," *IEEE Access*, vol. 7, pp. 160 263–160 273, 2019.
- [14] V. Valdivia, A. Barrado, A. La'zaro, M. Sanz, D. Lo'pez del Moral, and C. Raga, "Black-box behavioral modeling and identification of dc-dc converters with input current control for fuel cell power conditioning," *IEEE Trans. Ind. Electron.*, vol. 61, no. 4, pp. 1891–1903, 2014.
- [15] F. Alonge, F. D'Ippolito, F. M. Raimondi, and S. Tumminaro, "Nonlinear modeling of dc/dc converters using the hammerstein's approach," *IEEE Trans. Power Electron.*, vol. 22, no. 4, pp. 1210–1221, 2007.
- [16] I. Cvetkovic, D. Boroyevich, P. Mattavelli, F. C. Lee, and D. Dong, "Non-linear, hybrid terminal behavioral modeling of a dc-based nanogrid system," in *2011 Twenty-Sixth Annual IEEE Applied Power Electronics Conference and Exposition (APEC)*, 2011, pp. 1251–1258.
- [17] A. Wunderlich and E. Santi, "Digital twin models of power electronic converters using dynamic neural networks," in *2021 IEEE Applied Power Electronics Conference and Exposition (APEC)*, 2021, pp. 2369–2376.

TABLE IX: Coefficient functions of the SPV impedance model.

Coefficient functions	$V_o^2$	$V_o^2 L$	$I_L^2 V_o$	$V_o^3$	$V_o^3 L$	$I_L^3 V_o$
$g_0(I_L, V_o)$	468706540	3402526958327	-7722431663479	0	-8954003756	3103861994
$g_1(I_L, V_o)$	-2273731272	4814284053	-10866628680	5985291	-12633285	4596746
$g_2(I_L, V_o)$	660.60	4830567	-10963631	0	-12712	4407
$g_3(I_L, V_o)$	-339.65	637.68	-1438.46	0.89	-1.67	0.61
$f_0(I_L, V_o)$	1605877346	20796125904300	-47200425924942	0	-54726594406	19039742507
$f_1(I_L, V_o)$	304184187	222580872432	-505174659343	0	-585738625	202944111
$f_2(I_L, V_o)$	-16986469	38244673	-86358936	44711	-100377	36466
$f_3(I_L, V_o)$	0.38	0	0	0	0	0

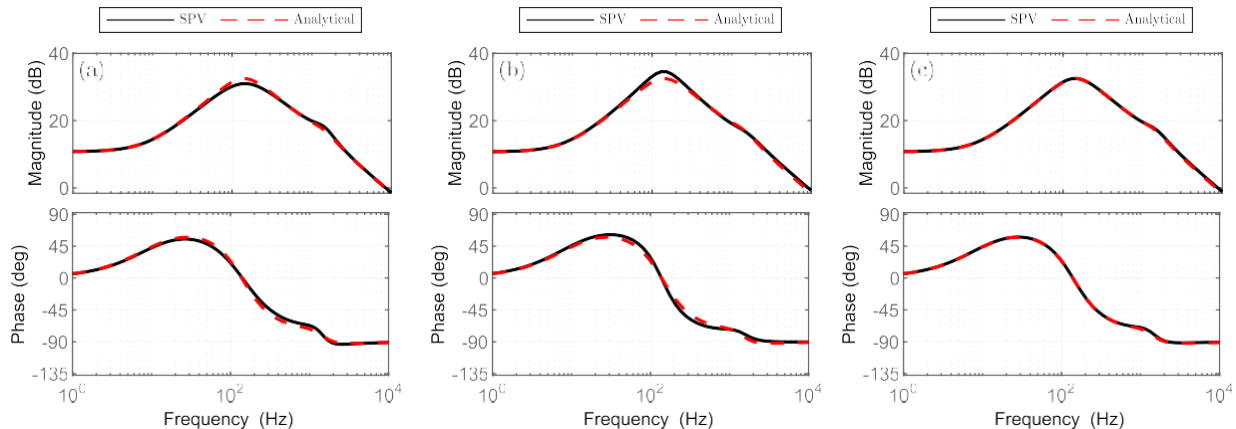


Fig. 13: Validation of the SPV impedance model against its analytical counterpart at (a)  $V_o = 369.7$  V,  $I_L = 4.4$  A (b)  $V_o = 383.4$  V,  $I_L = -1.5$  A (c)  $V_o = 376.2$  V,  $I_L = 1.6$  A.

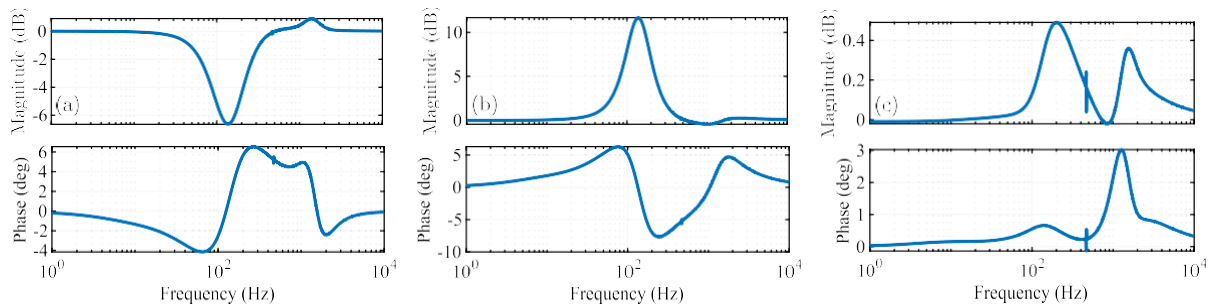


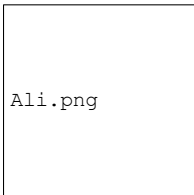
Fig. 14: Identification error of the SPV impedance model at (a)  $V_o = 369.7$  V,  $I_L = 4.4$  A (b)  $V_o = 383.4$  V,  $I_L = -1.5$  A (c)  $V_o = 376.2$  V,  $I_L = 1.6$  A.

- [18] A. France's, R. Asensi, Garc'ia, R. Prieto, and J. Uceda, "Modeling electronic power converters in smart dc microgrids—an overview," *IEEE Trans. Smart Grid*, vol. 9, no. 6, pp. 6274–6287, 2018.
- [19] L. Aguirre, P. Donoso-Garcia, and R. Santos-Filho, "Use of a priori information in the identification of global nonlinear models—a case study using a buck converter," *IEEE Trans. Circuits Syst. I*, vol. 47, no. 7, pp. 1081–1085, 2000.
- [20] M. Correa, L. Aguirre, and R. Saldanha, "Using steady-state prior knowledge to constrain parameter estimates in nonlinear system identification," *IEEE Trans. Circuits Syst. I*, vol. 49, no. 9, pp. 1376–1381, 2002.
- [21] F. Hafiz, A. Swain, E. M. A. M. Mendes, and L. A. Aguirre, "Multiobjective evolutionary approach to grey-box identification of buck converter," *IEEE Trans. Circuits Syst. I*, vol. 67, no. 6, pp. 2016–2028, 2020.
- [22] J. A. Oliver, R. Prieto, J. A. Cobos, O. Garcia, and P. Alou, "Hybrid wiener-hammerstein structure for grey-box modeling of dc-dc converters," in *2009 Twenty-Fourth Annual IEEE Applied Power Electronics Conference and Exposition*, 2009, pp. 280–285.
- [23] S. Zhao, Y. Peng, Y. Zhang, and H. Wang, "Parameter estimation of power electronic converters with physics-informed machine learning," *IEEE Trans. Power Electron.*, pp. 1–1, 2022.
- [24] R. Xu, Z. Zou, J. Tang, X. Liu, Y. Zhang, and C. Xu, "Stability analysis of power converter-based constant power load with reduced-order model," *IEEE J. Emerg. Sel. Topics Ind. Electron.*, vol. 4, no. 3, pp. 756–766, 2023.
- [25] S. Shah, P. Koralewicz, V. Gevorgian, H. Liu, and J. Fu, "Impedance methods for analyzing stability impacts of inverter-based resources: Stability analysis tools for modern power systems," *IEEE Electr. Mag.*, vol. 9, no. 1, pp. 53–65, 2021.
- [26] H. Abdollahi, A. Khodamoradi, E. Santi, and P. Mattavelli, "Online bus impedance estimation and stabilization of dc power distribution systems: A method based on source converter loop-gain measurement," in *2020 IEEE Applied Power Electronics Conference and Exposition (APEC)*, 2020, pp. 3371–3378.
- [27] R. Hassan, H. Wang, and R. Zane, "Continuous stability monitoring of dc microgrids using controlled injection," in *2019 IEEE Applied Power Electronics Conference and Exposition (APEC)*, 2019, pp. 1357–1364.
- [28] A. Khodamoradi, H. Abdollahi, E. Santi, and P. Mattavelli, "A loop gain-based technique for online bus impedance estimation and damping in dc microgrids," *IEEE Trans. Power Electron.*, vol. 36, no. 8, pp. 9648–9658, 2021.
- [29] L. Fan, Z. Miao, P. Koralewicz, S. Shah, and V. Gevorgian, "Identifying dq-domain admittance models of a 2.3-mva commercial grid-following inverter via frequency-domain and time-domain data," *IEEE Trans. Energy Convers.*, vol. 36, no. 3, pp. 2463–2472, 2021.
- [30] M. Zhang, X. Wang, D. Yang, and M. G. Christensen, "Artificial neural

- network based identification of multi-operating-point impedance model,” *IEEE Trans. Power Electron.*, vol. 36, no. 2, pp. 1231–1235, 2021.
- [31] M. Zhang, Q. Xu, and X. Wang, “Physics informed neural network based online impedance identification of voltage source converters,” *IEEE Trans. Ind. Electron.*, pp. 1–1, 2022.
- [32] S. L. Brunton, J. L. Proctor, and J. N. Kutz, “Discovering governing equations from data by sparse identification of nonlinear dynamical systems,” *Proceedings of the National Academy of Sciences*, vol. 113, no. 15, pp. 3932–3937, 2016.
- [33] U. Fasel, E. Kaiser, J. N. Kutz, B. W. Brunton, and S. L. Brunton, “Sindy with control: A tutorial,” *arXiv preprint arXiv:2108.13404*, 2021.
- [34] L. Zhang and H. Schaeffer, “On the convergence of the sindy algorithm,” *Multiscale Modeling & Simulation*, vol. 17, no. 3, pp. 948–972, 2019.
- [35] M. K. Kazimierczuk, *Pulse-width modulated DC-DC power converters*. John Wiley & Sons, 2015.
- [36] A. Hosseinipour and H. Hojabri, “Small-signal stability analysis and active damping control of dc microgrids integrated with distributed electric springs,” *IEEE Trans. Smart Grid*, vol. 11, no. 5, pp. 3737–3747, 2020.
- [37] R. Pintelon and J. Schoukens, *System identification: a frequency domain approach*. John Wiley & Sons, 2012.
- [38] A. Riccobono and E. Santi, “Comprehensive review of stability criteria for dc distribution systems,” in *2012 IEEE Energy Conversion Congress and Exposition (ECCE)*, 2012, pp. 3917–3925.

**Ali Hosseinipour** (S’21) received the B.S. and M.S. degrees in electrical engineering from Shahid Bahonar University of Kerman, Iran.


He is currently pursuing the Ph.D. in electrical engineering at the Electrical and Computer Engineering Department at Lehigh University, PA, USA. His research interests include dynamic modeling and control of modern power systems and microgrids. He is the recipient of the 3rd Prize at 2023 IEEE PESGM graduate student poster contest for his work on data-driven impedance modeling of power converters in microgrids..



Ali.png

converters in microgrids..

**Javad Khazaei** (S’10 M’16 SM’20) received the Ph.D. degree in Electrical Engineering from University of South Florida (USF) in 2016 with focus on power and energy systems. He is currently an Assistant Professor at the Electrical and Computer Engineering Department at Lehigh University, PA, USA. His research interests include data-driven and model-based control, optimization, and dynamic modeling of cyber-physical power systems and microgrids, smart grid security, and power electronics applications in smart grids and shipboard microgrids.



Javad.jpg